Ultrasonics Sonochemistry 72 (2021) 105445

Contents lists available at ScienceDirect

Ultrasonics Sonochemistry

journal homepage: www.elsevier.com/locate/ultson

Effects of sonochemical approach and induced contraction of core–shell bismuth sulfide/graphitic carbon nitride as an efficient electrode materials for electrocatalytic detection of antibiotic drug in foodstuffs

Mani Govindasamy [a], Sea-Fue Wang [a,*], Albandary Almahri [b,*], U. Rajaji [c]

[a] Department of Materials and Mineral Resources Engineering, NTUT, No. 1, Sec. 3, Chung-Hsiao East Rd., Taipei 106, Taiwan, ROC
[b] General Courses Unit, Faculty of Sciences and Arts, King Khalid University, Dhahran Aljanoub, Saudi Arabia
[c] Department of Chemistry, Bishop Heber College, Tiruchirappalli, Tamil Nadu 620017, India

ARTICLE INFO

Keywords:
Electrocatalyst
Sonochemical reactions
Cyclic voltammetry
Antibiotic drug
Electrochemical detection

ABSTRACT

Ultrasonic-enhanced surface-active bismuth trisulfide based core–shell nanomaterials were developed and used as an efficient modified electrode material to construct a highly sensitive antibiotic sensor. The core–shell Bi_2S_3@GCN electrode material was directly synthesized by in-situ growth of GCN on Bi_2S_3 to form core–shell like nanostar (Ti-horn, 30 kHz, and 70 W/cm^2). The electrocatalyst of Bi_2S_3@GCN nanocomposites was efficaciously broadened towards electrochemical applications. As synthesized Bi_2S_3@GCN promoted the catalytic ability and electrons of GCN to transfer to Bi_2S_3. The single-crystalline GCN layers were uniformly grown on the surface of the Bi_2S_3 nanostars. Under the optimal conditions of electrochemical analysis, the CPL sensor exhibited responses directly proportional to concentrations (toxic chemical) over a range of 0.02–374.4 μM, with a nanomolar detection limit of 1.2 nM (signal-to-noise ratio S/N = 3). In addition, the modified sensor has exhibited outstanding selectivity under high concentrations of interfering chemicals and biomolecules. The satisfactory CPL recoveries in milk product illustrated the credible real-time application of the proposed Bi_2S_3@GCN sensors for real samples, indicating promising potential in food safety department and control. Additionally, the proposed electrochemical antibiotic sensor exhibited outstanding performance of anti-interfering ability, high stability and reproducibility.

1. Introduction

The sonochemical technique has been demonstrated to be an environmentally and eco-friendly method to obtain novel nanomaterials and composites [1]. The sonochemical and ultrasound approaches have been manifested as a non-toxic and green synthesis method to obtain novel electrocatalyst. Hence, the sonochemical effects of ultrasonic irradiation emerge from acoustic cavitation's [1,2]. In particularly, the formation, and growth of the nanoparticles based on the implosive collapse of bubbles in a reaction medium, which reaction results in an instantaneously low temperature and pressure pulse [3]. Therefore, these significant advantages of the sonochemical approaches lead to many unique nanomaterials in the irradiated solution [4]. In particular, bimetal sulfides with general formula A_2S_3 (A = Co, Fe, Ni, Mn, Bi, Al) have attracted considerable attention in chemical sensing and development of electrochemical devices on account of their semiconductive properties [5,6]. Among the various bimetal sulfides, the n-type semiconductor, Bismuth sulfide (Bi_2S_3), with a direct band gap (Eg = 1.3 to 1.7 eV), has gained a substantial interest in electrochemistry due to its high natural abundance, excellent photovoltaic properties, and favorable compatibility with the environment [7,8]. Generally, n-type crystalline semiconductor material use electron as majority carriers owing to the high availability of electrons than holes. Bi_2S_3 can be synthesized in various morphology and size, such as one-dimensional nanoribbons, nanorods, nanowires, and nanotubes using various synthesis methods [9,10] including hydrothermal/solvothermal decomposition [11], sonochemical [3], microwave irradiation [8], and vapor deposition which offers significant improvement in the physical properties and better efficiency in electrochemical field [11,12]. It is to be noted that Bi_2S_3 nanostructure is normally aggregated during growth processes, which not only decreases the effective surface area, but also greatly limits the electrochemical performance with low sensitivity, limited

* Corresponding authors.
E-mail addresses: govindasamy420700@gmail.com (M. Govindasamy), sfwang@ntut.edu.tw (S.-F. Wang), almohry@kku.edu.sa (A. Almahri).

https://doi.org/10.1016/j.ultsonch.2020.105445
Received 24 January 2020; Received in revised form 16 December 2020; Accepted 19 December 2020
Available online 24 December 2020

detection limit, and wide linear range. Hence, it is significant to combine Bi_2S_3 with carbonaceous materials to develop novel nanocomposite to further boost the electrode efficiency. Graphitic carbon nitride (g-C_3N_4) is a unique choice amongst the available carbon-based materials due to its fascinating physical properties [13,14]. The carbon allotrope, g-C_3N_4 with its stacked two-dimensional structure and semiconducting properties has gained a remarkable impact in development of electrochemical sensors. Related investigations reveal that it has been effectively used in gas sensors, photocatalytic degradation, and as electrochemical sensor owing to its excellent thermal stability, tunable electronic structures, high electronic conductivity, and unique electronic property with low-cost and non-toxicity [15–17]. The layered polymeric structure of g-C_3N_4 offers high surface area, electron transfer channels, and active site which makes it a favorable material in electrochemistry. In this present study, a novel incorporation of Bi_2S_3 with g-C_3N_4 (GCN) through facile sonochemical method is demonstrated. The detection of chloramphenicol with Bi_2S_3@GCN as a modified screen-printed carbon electrode (SPCE) exhibits excellent sensitivity, specificity, and selectivity with wide linear range and lower limit of detection (Scheme 1).

Chloramphenicol (CPL) is an antibiotic with broad active spectrum which is extensively employed in aquaculture against the gram-negative and gram-positive bacteria [18–20]. Scientific investigations have revealed its effectivity in treating life-threatening diseases such as typhoid fever and childhood meningitis and septicaemia. However, the use of CPL has been restricted owing to its toxicity and excessive usage which causes gray-baby syndrome, aplastic anemia, and bone-marrow suppression [19,21]. Although certain restrictions were imposed in the usage of CPL by some nations, its out-and-out eradication is difficult by virtue of its application in wide range of production process, low-cost, and high availability [22,23]. The countries like China, Canada, USA, European Union, and Japan have banned the usage of CPL in the production of animal food. In 2002, the European Union proposed ban on CPL in shrimp products from China for the duration of 30 months [24–26]. The USA has also banned CPL due to the former causes; both cases adversely affected the economy of China-based CPL products in 2006 [27]. The maximum permissible level of CPL in milk is set as 0.3 ppb. Hence, the efficient detection of CPL using a rapid, cost-effective, and ultrasensitive method is highly significant. Different techniques including bioassay method, HPLC [28], immunoassay, and gas chromatography-tandem mass spectrometry were employed to analyze the CPL level in food products [28–30]. However, aforementioned techniques have several drawbacks such as high-cost, long-processing time, and need for trained professional to carry out the experiments. In order to overcome these drawbacks, electrochemical method is employed in this work as it possess various advantages such as rapid detection, high specificity, low-cost, compact instrumental size, and fast response.

2. Experimental section

2.1. Sonochemical synthesis of Bi_2S_3/GCN

In this typical synthesis given briefly, 0.05 mol of bismuth(III) nitrate pentahydrate ($Bi(NO_3)_3{\cdot}5H_2O$), 0.1 mol of triethanolamine (TEA), and 0.02 mol of sodium thiosulfate ($Na_2S_2O_3$) were mixed in 50 mL

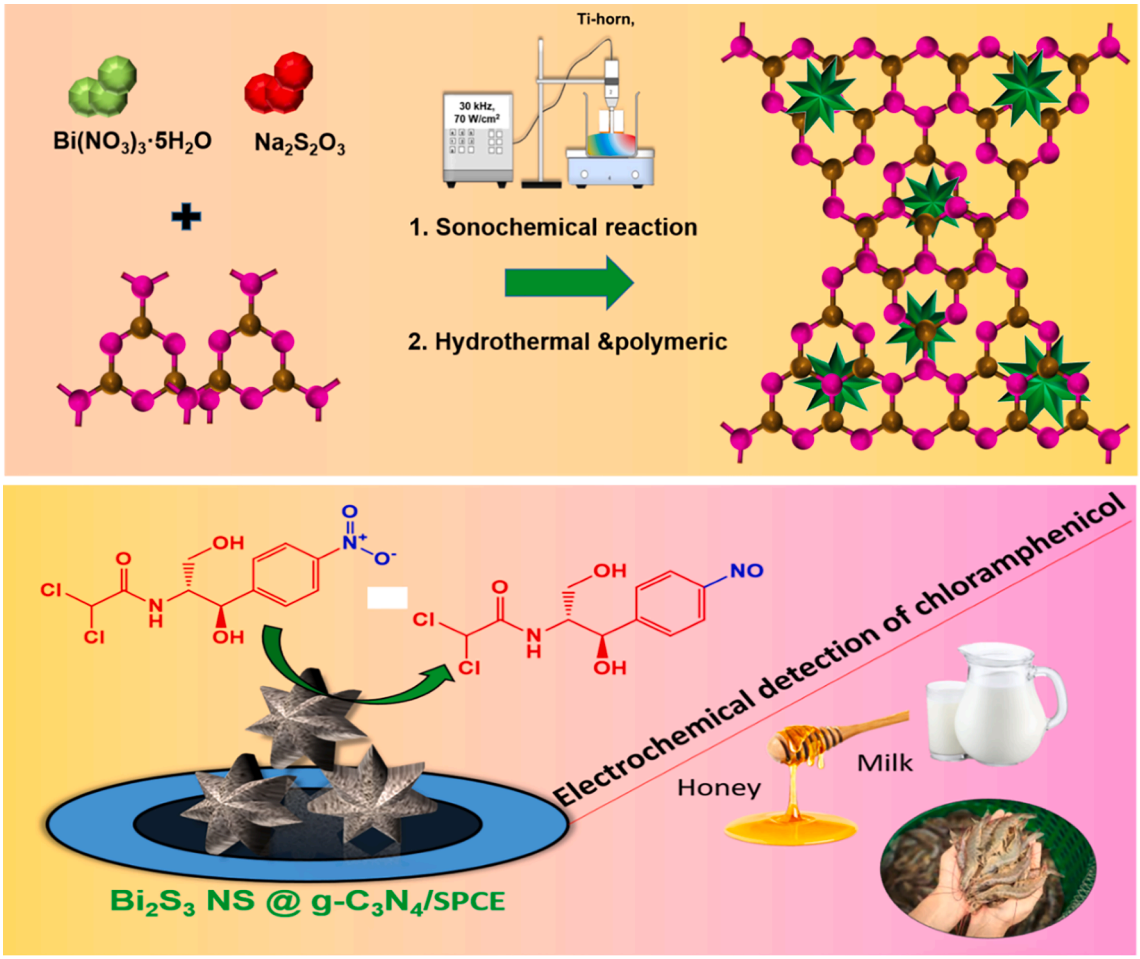

Scheme 1. Schematic diagram of the electrochemical sensor and its applications.

deionised water and the solution was stirred under magnetic stirrer. Then, the mixture of the solution was moved to high-intensity ultrasound irradiation under ambient air for 2 h. This ultrasound irradiation was provided using a high-intensity ultrasonic probe (model name: Xinzhi Co.; 0.6 cm diameter; Ti-horn, 30 kHz, and 70 W/cm^2) immersed directly in the mixture of the solution under the room temperature. We obtained the precipitates after 2 h of sonochemical reaction. Then, the resultant precipitates were washed through centrifugation method, using 0.1 mol HCl, deionised water, and ethanol. Afterwards, the product was dried in vacuum oven at 55 °C (Scheme 2).

0.2 g of melamine and 0.1 g of Bi_2S_3 particles were added in 50 mL of deionized water under magnetic stirring at 80 °C for 15 min. Then, the reaction solution was transferred into a 100 mL Teflon-stainless autoclave and heated at 180 °C for 2 h in an oven. Afterwards, the obtained precipitates were washed with denoised water and the melamine-cyanuric acid complex/Bi_2S_3 was heated at 550 °C for 5 h with a heating rate of 5 °C/min under nitrogen atmosphere to obtain Bi_2S_3/GCN composite as the final product.

2.2. Fabrication of Bi_2S_3@GCN hybrid modified electrode

Prior to the modification of screen-printed carbon electrode (SPCE) with Bi_2S_3@GCN hybrid, we thoroughly washed the SPCE surface using water and ethanol to remove any impurities if present. Then, the SPCE was dried at room temperature. Afterwards, 8 μL of Bi_2S_3@GCN hybrid (5 mg/mL) was drop casted over the surface of SPCE. The Bi_2S_3@GCN hybrid modified SPCE was then dried at room temperature. Ultimately, Bi_2S_3@GCN hybrid/SPCE was developed and used for electrochemical detection of CPL.

3. Results and discussion

3.1. XRD and XPS analysis of Bi_2S_3@GCN hybrid

The XRD patterns of the Bi_2S_3@GCN was displayed in Fig. 1A. The XRD analysis of Bi_2S_3@GCN shows sharp diffraction peaks correlated to (200), (120), (220), (101), (310), (211), (221), (410), (311), (240), (430), (421), (440), (501), (160), (312), (360), (640), (152), (721), (532), (651), (811), and (213) planes. These diffraction patterns were matched with the orthorhombic Bi_2S_3@GCN (JCPDS No. 01-084-0279) [31,32]. Moreover, the XRD peaks and JCPDS card indicates the successful formation of Bi_2S_3 particles. In addition, the graphitic carbon nitride (GCN) has exhibited the diffraction peaks at 11.02° and 24.15° corresponding to the Miller indices planes (100) and (002) [33]. These observations from the XRD analysis of Bi_2S_3@GCN composite confirms the successful hybrid formation. Crystal structure of the Bi_2S_3 nanoparticles were analyzed and given in Scheme 3. The Bi_2S_3 particles have orthorhombic crystal structure and unit cell volume is 502.28 Å^3. Further details regarding orthorhombic crystal structure is given in supporting information.

Fig. 2B-F, displays XPS measurements to evaluate the chemical state of as-synthesized core-like Bi_2S_3@GCN nanostructures. The survey spectrum as shown in Fig. 1B, reveals that as-synthesized core-like Bi_2S_3@GCN nanostructures exhibits peaks of Bi 4f, S 2p, C 1s, and N 1s. Fig. 1C depicts a high resolution Bi 4f XPS of the composite, typically comprised of doublet binding energies at ~157.3 eV (Bi $4f_{5/2}$) and ~163.4 eV (Bi $4f_{3/2}$), which normally ascribe to the oxidation state of Bi^{3+} [34]. Fig. 1D displays two binding energy peaks at ~157.2 eV and ~163.1 eV corresponding to S $2p_{3/2}$ and S $2p_{1/2}$ respectively [35]. There are mainly GCN based carbon bonds present in the C 1s spectrum (Fig. 1E) and the important binding energies are obtained to be 284.8 eV, 286.4, and 288.1 eV. It is to be noted that the low intensity peak at 286.4 eV is assigned to the C–NH_2 energy of the GCN [36,37]. The peak at lower binding energy (BE), centered at 284.8 eV, is attributed to C–C/C=C bonds and the peak at 288.1 eV is attributed to N-C=N based sp^2 bonds of the GCN ring system. The N 1s core level spectra show a sharp peak centered at 399.3 eV with a shoulder at higher binding energy (Fig. 1F). Deconvolution of the data for the Bi_2S_3@GCN composite reveals contributions of four peaks at 398.5, 399.3, 401.0, 404.5 eV, respectively [37]. Therefore, the XPS analysis and its results were confirming the presence of Bi_2S_3@GCN composite.

3.2. Morphological analysis of Bi_2S_3@GCN composite

Transmission electron microscopy (TEM) technique was used to conduct surface analysis to elucidate the structure and morphology of the applied nanomaterials. As observed in Fig. 2A-C, the layered GCN was loaded on nanostars of Bi_2S_3. Moreover, energy dispersive X-ray analysis (EDS) of Bi_2S_3@GCN (Fig. 2B) revealed the existence of the elements including Bi, S, C and N, providing additional evidence for the

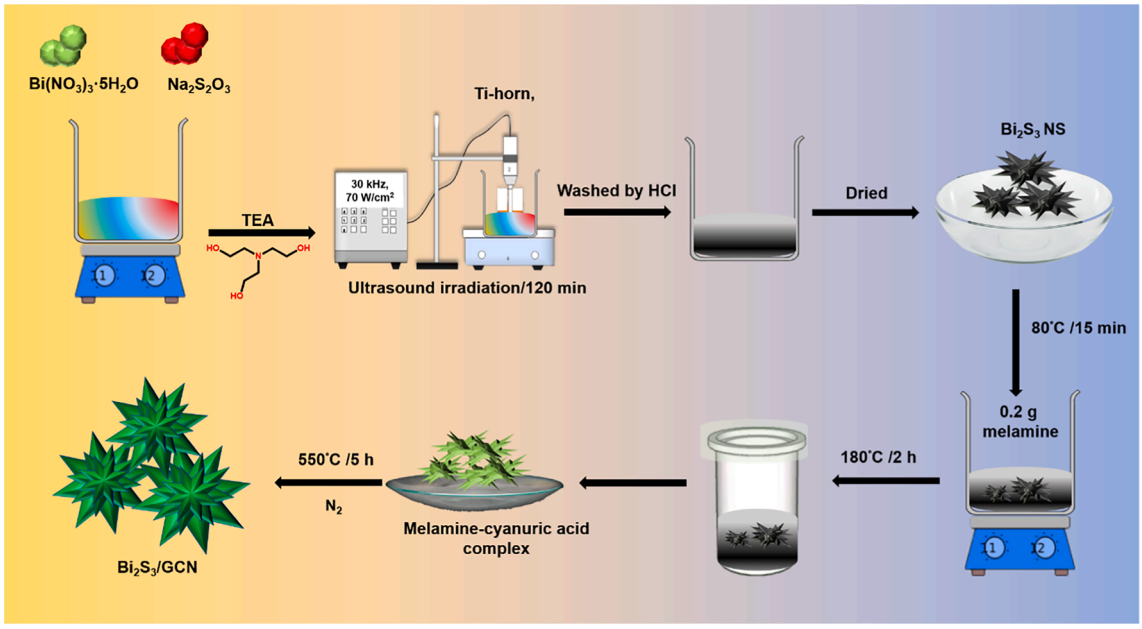

Scheme 2. Determination of chloramphenicol (CPL) in food samples using Bi_2S_3@GCN hybrid modified SPCE.

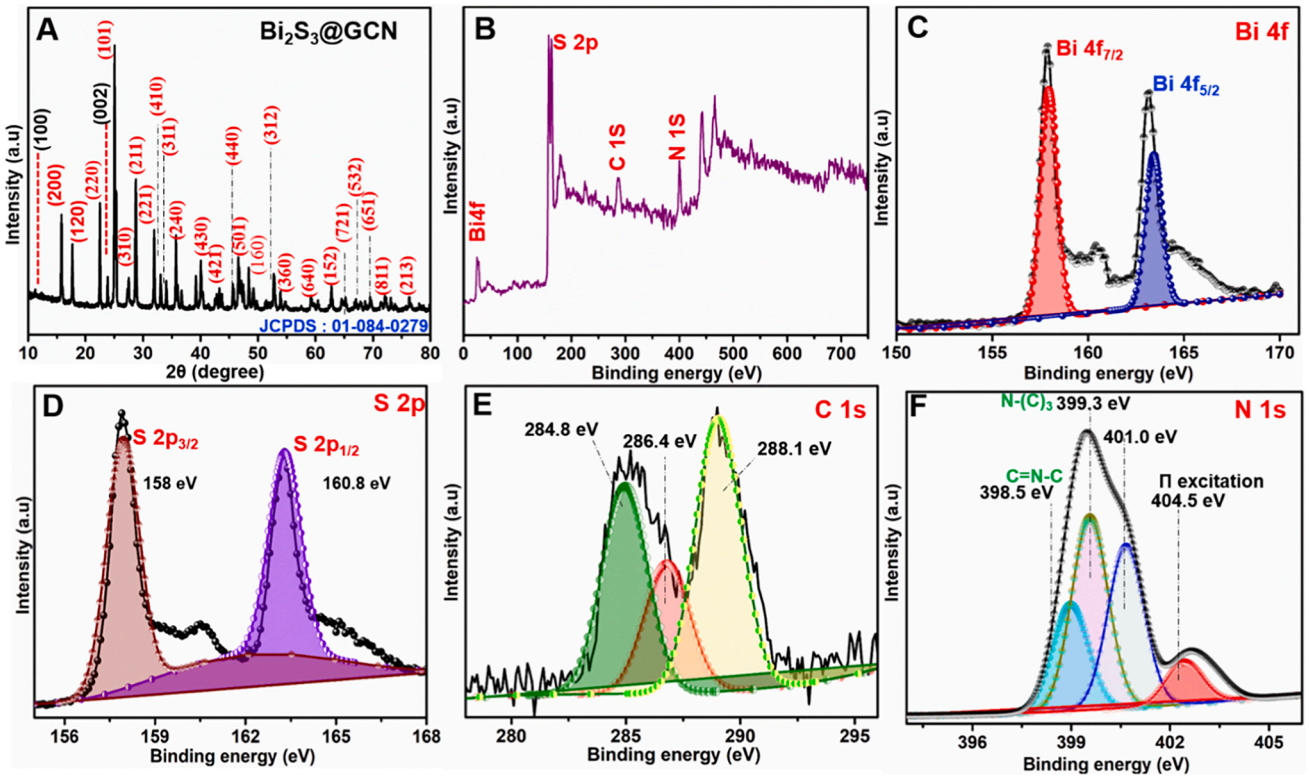

Fig. 1. XRD analysis of Bi_2S_3@GCN (A) and XPS survey analysis of Bi_2S_3@GCN (B). High resolution and conventional analysis of Bi 4f (C), S 2p (D), C 1s (E), N1s (F).

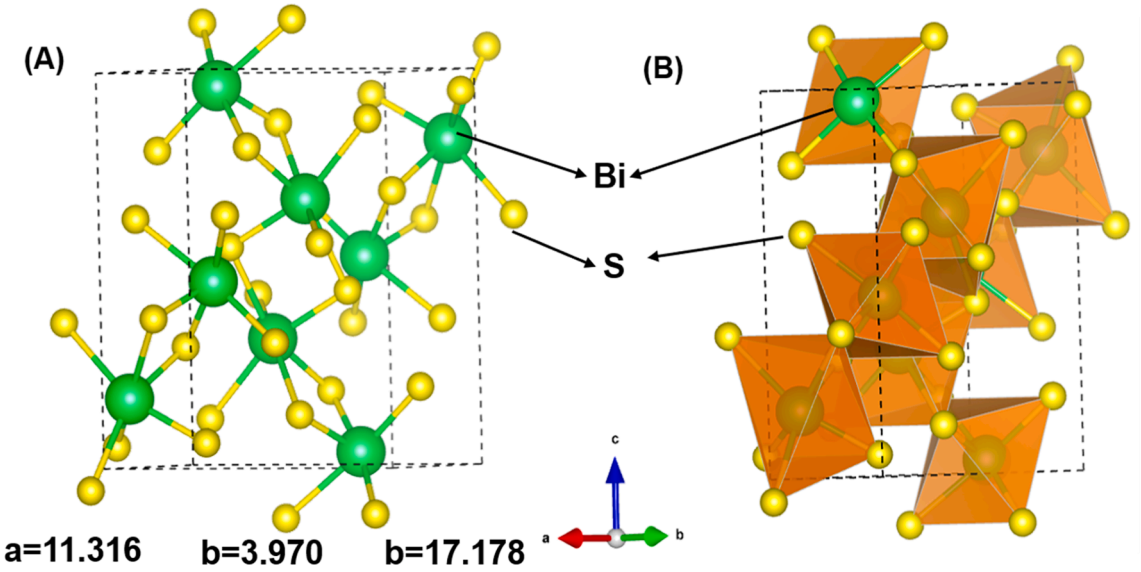

Scheme 3. Crystal structure analysis of Bi_2S_3 nanoparticle (A) ball-stick model and polyhedral model.

successful synthesis of Bi_2S_3@GCN. Fig. 2E-H shows the elemental mapping in scanning transmission electron images of Bi_2S_3@GCN which shows that a large number of graphitic carbon nitrides were covered on the surface of Bi_2S_3. The successful formation of the Bi_2S_3@GCN composite as a core–shell electrode material is evident from the obtained results.

3.3. Electrochemical characterization of the core–shell Bi_2S_3@GCN/SPCE

The electro-conductivity and resistance measurement are often used to study the electron transfer ability of bare SPCE and modified SPCE. The EIS analysis and spectra of Bi_2S_3/SPCE, GCN/SPCE, Bi_2S_3@GCN/SPCE, and unmodified SPCE in 5 mM $[Fe(CN)_6]^{3-/4-}$ containing 0.1 M potassium chloride is shown in Fig. 3. The Randles equivalent circuit was used to fit the spectra to obtain good semicircles. The elements of the circuit are presented like C_d – the double-layer Capacitance, R_{ct} – the charge transfer resistance, R_s – the solution resistance and Z_W – the impedance of Warburg [22,38]. The charge transfer resistance values were calculated for the unmodified electrode (136.5 Ω), Bi_2S_3/SPCE (77.2 Ω), GCN/SPCE (56.2 Ω), and Bi_2S_3@GCN/SPCE (33.1 Ω). These data expressed clearly and proved that the Bi_2S_3@GCN/SPCE is an

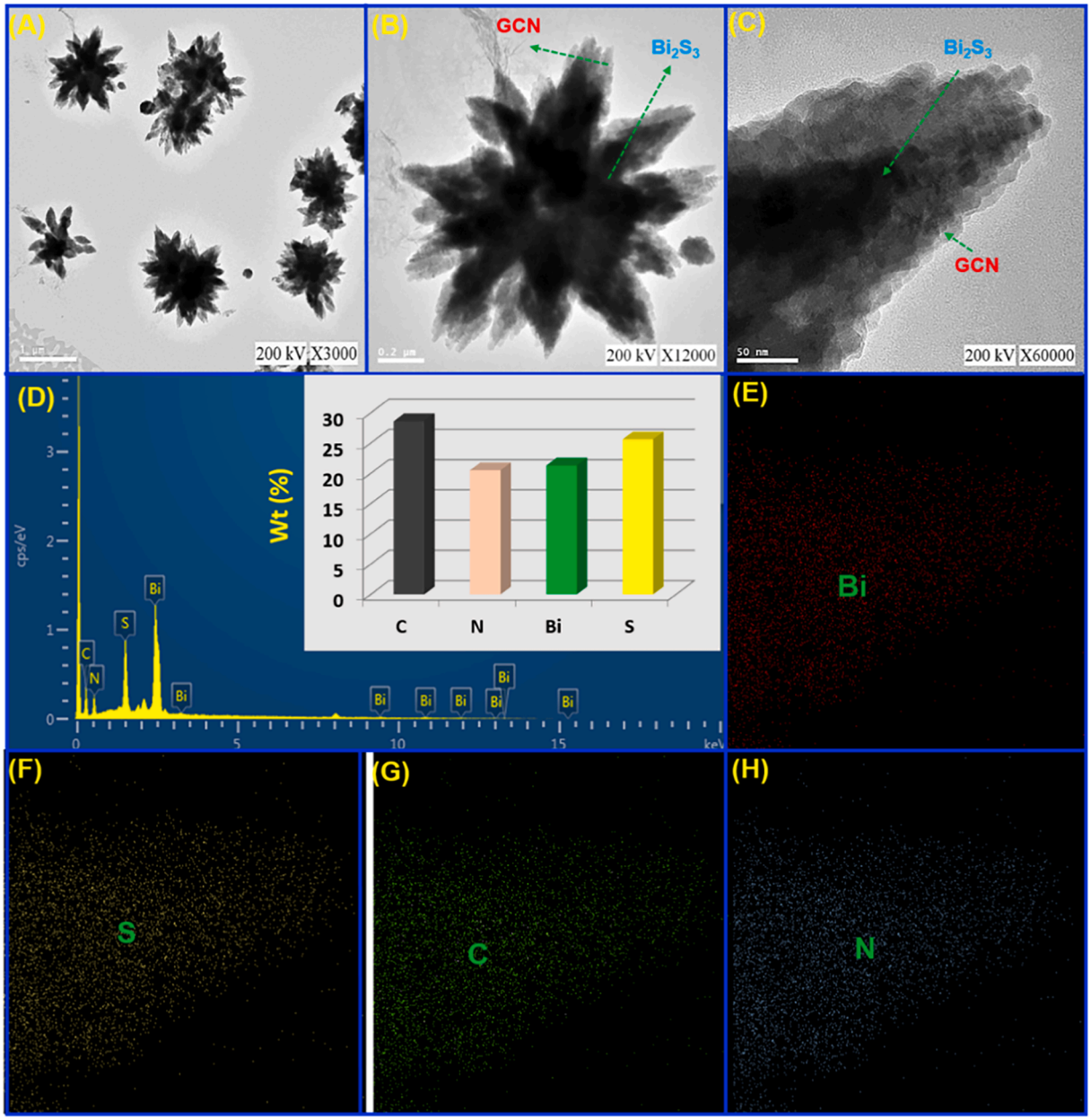

Fig. 2. TEM analysis of Bi_2S_3@GCN hybrid (A-C), elemental analysis and quantitative analysis of Bi_2S_3@GCN (D), elemental mapping analysis of the hybrid material (E-H).

electrode material with good electric based properties for the electrochemical sensing applications towards CPL.

3.4. *Electrochemical optimization at core–shell Bi_2S_3@GCN/SPCE*

The effect of catalyst concentration of the Bi_2S_3@GCN material was analyzed. The current reduction increases with the suspension concentration increasing from 2 to 8 mg/mL. Nevertheless, the catalyst concentration of the Bi_2S_3@GCN composite exhibits higher performance in 5 mg/mL. Consequently, 5 mg/mL of the Bi_2S_3@GCN composite was used as the optimal catalyst concentration. The amount of Bi_2S_3@GCN catalyst concentration on the SPCE plays a major role in the electrochemical reduction of CPL detection (sensor). With an increase in the Bi_2S_3@GCN catalyst volume from 5.0 to 10.0 μL, the reduction current for CPL increased. The further increase in the Bi_2S_3@GCN catalyst concentration to 9.0 μL resulted in a significant decrease in the CPL reduction performance. Therefore, 8.0 μL was selected as the optimal volume and was applied in all electrochemical experiments carried out in this work.

The voltammetric technique was applied to analyze the effect of pH conditions on the electrocatalytic activity of CPL at a scan rate of 0.05 V/s, as shown in Fig. 4A. It can be observed that the reduction peak current increases with an increase in pH from pH 3.0 to pH 7.0. Further, it can be noted that beyond pH 7.0, the reduction peak current decreased gradually. Moreover, the peak reduction potential of CPL shifted more towards negative value when the pH is increased from pH 3.0 to pH 11.0 (Fig. 4B). Furthermore, pH 7.0 is a biological pH value and it could be potentially used in various biological and medical fields. Hence, pH 7.0 was selected as the optimal pH of the supporting electrolyte in the electrochemical analysis of Bi_2S_3@GCN/SPCE toward the determination of CPL.

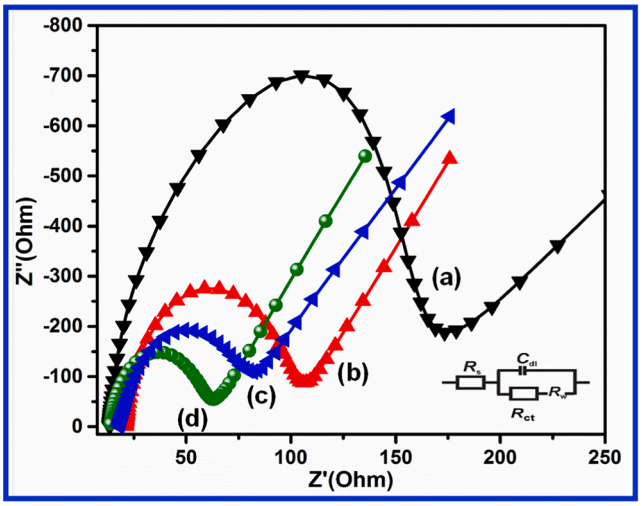

Fig. 3. EIS (interface properties) analysis of SPCE (a), Bi_2S_3/SPCE (b), GCN/SPCE (c), Bi_2S_3@GCN hybrid/SPCE (d).

3.5. Electrochemical detection of CPL at core–shell Bi_2S_3@GCN/SPCE by CV method

The electrochemical responses of CPL at Bi_2S_3@GCN/SPCE was estimated and compared to those obtained at bare SPCE, Bi_2S_3/SPCE, and GCN/SPCE. Therefore, voltammetric analysis was performed for different electrodes such as bare SPCE, Bi_2S_3/SPCE, GCN/SPCE, and Bi_2S_3@GCN/SPCE with CPL (100 μM) in saturated N_2 containing phosphate buffer (pH 7) at 50 mV s^{-1}. The obtained voltammograms are given in Fig. 5A. It can be observed that the CV curve of bare SPCE showed a very small cathodic response (I_{pc}) for CPL concentration (pH 7.0). Similarly, Bi_2S_3/SPCE and GCN/SPCE also exhibited a small cathodic peak response. Whereas, Bi_2S_3@GCN modified SPCE (d) showed a sharp and intense cathodic peak response of CPL drug at −0.72 (R_1). This peak response of the composite modified electrode is many folds higher than bare SPCE, Bi_2S_3/SPCE, and GCN/SPCE. Therefore, the obtained electrochemical results are evidently confirming that the synergetic effect of the Bi_2S_3 nanopartices and graphitic carbon nitride is not only enhancing the electro-conductivity of Bi_2S_3@GCN nanocomposite, but also improving its electrocatalytic (chemical) ability. The reduction peak (R_1) is fast reaction and it is ascribed as the change in nitrophenyl function group to hydroxylamine form based on nitro reduction mechanism. The electrochemical mechanism involving this four-electron transfer reaction is provided in Fig. 5E [23,39].

Fig. 5B shows the CV response of Bi_2S_3@GCN/SPCE for varying the concentration of CPL from 10 to 100 μM in nitrogen gas saturated 0.05 M phosphate buffer (pH 7.0) at a scan rate of 50 mV s^{-1}. The electrochemical performances and enhanced electrocatalytic properties of Bi_2S_3@GCN modified SPCE can be understood by exploring the linear increment in the cathodic peak current for the linear addition of CPL concentration. In addition, the linear calibration analysis of electrochemical reduction peak current vs. concentration of CPL drug is shown in Fig. 5B (inset) and the resultant linear regression equation of the plot is I_{pc} (μA) = 1.2 μM + 8.08 (R^2 = 0.9767). This result more evidently confirms that Bi_2S_3@GCN/SPCE is a promising modified electrode material for efficient electro-catalytic detection of CPL drug without any fouling effect. The electrochemical response of CPL drug Bi_2S_3@GCN/SPCE was evaluated under different scan rates at same electrochemical conditions. Fig. 5C shows the voltammetric response of Bi_2S_3@GCN/SPCE for CPL drug (50 μM) in nitrogen gas saturated 0.05 M phosphate buffer (pH 7.0) at various scan rates from (peaks; a-o) 20 to 300 mV s^{-1}. The corresponding calibration plot of reduction peak current vs. square root of the scan rate with R^2 = 0.9959, was shown in Fig. 5D. These results indicate that the overall electrochemical reduction process of CPL drug at Bi_2S_3@GCN/SPCE is a diffusion-controlled reaction.

3.6. Electrochemical determination of CPL at core–shell Bi_2S_3@GCN/SPCE by differential pulse voltammetry (DPV)

DPV technique is applied to analyze the sensitivity, linear range, and limit of detection (LOD) of electrochemical performance of Bi_2S_3@GCN modified SPCE towards CPL detection. DPV is considered as a highly sensitive and robust analytical technique to determine the important electrochemical parameters and electrocatalytic ability of the modified electrodes. Consequently, DPV method was used for CPL detection based on Bi_2S_3@GCN modified SPCE in nitrogen gas saturated 0.05 M phosphate buffer (pH 7.0). Fig. 6A shows the voltammetric peaks with the linear increment of reduction peak response over the concentration of CPL drug from 0.02 μM to 374.4 μM. Furthermore, the linearity-based equation for the obtained calibration plot is I_{pc} (μA) = 1.536–2.26C (μM) and the R^2 is 0.9912 (Fig. 6B). In addition, the modified electrode sensitivity of the sensor was calculated and is 85.33 μA μM^{-1} cm^{-2} and it has calculated from the slope of the calibration plot/surface area (0.018 cm^2) of the electrode. Further, the LOD of CPL drug at Bi_2S_3@GCN/SPCE was calculated and is 0.0012 μM (1.2 nM) and the limit of quantification was calculated to be 20 nM. Moreover, the electrochemical parameters of LOD, sensitivity, and linear range of CPL drug at Bi_2S_3@GCN/SPCE were compared with previously reported electrochemical sensor based modified electrodes as given in Table 1. According to the comparison Table 1, Bi_2S_3@GCN modified SPCE has achieved very low detection

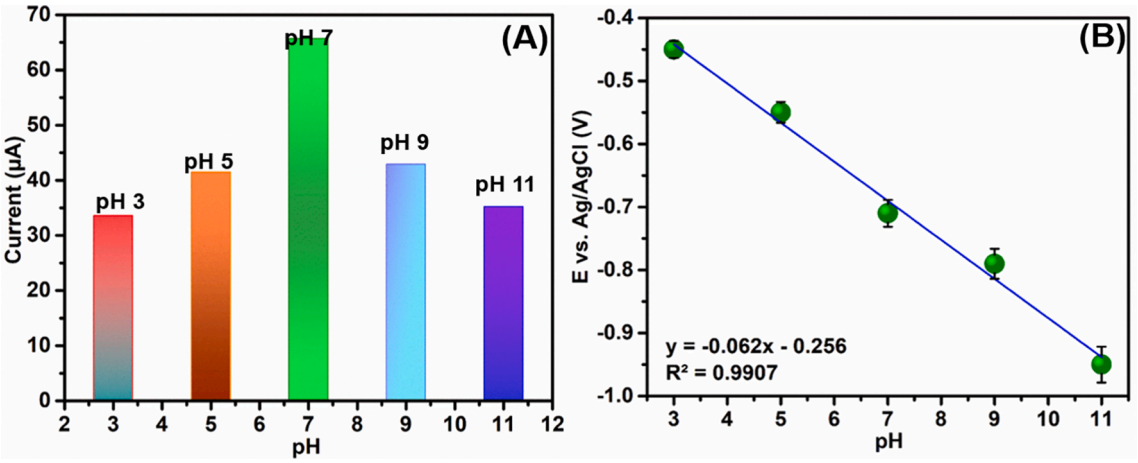

Fig. 4. (A and B) Different pH analysis of CPL (100 μM) at Bi_2S_3@GCN hybrid modified SPCE (50 mV/s.

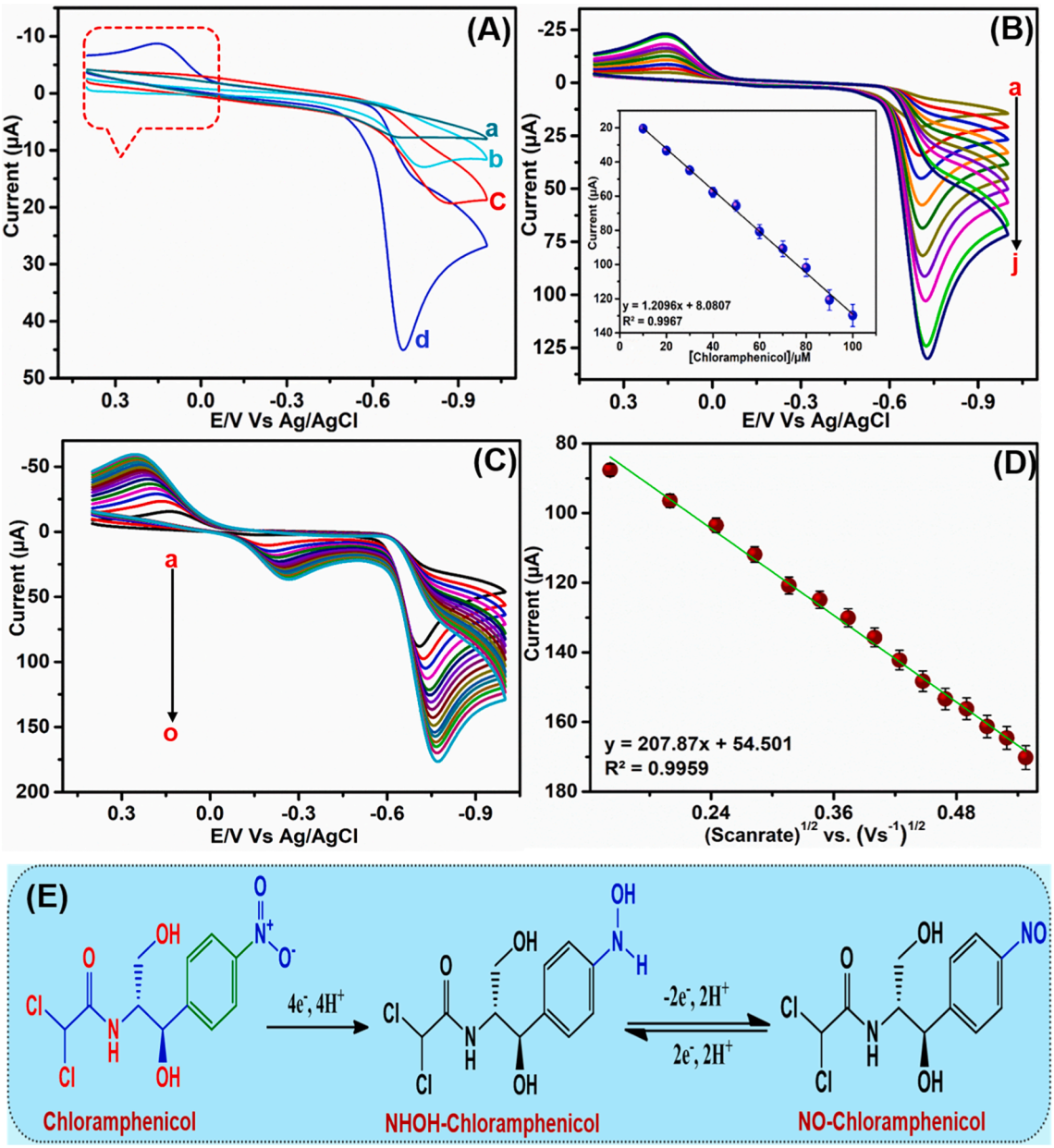

Fig. 5. (A) CV analysis of unmodified SPCE (a), Bi_2S_3 NPs/SPCE (b), GCN/SPCE (c), Bi_2S_3@GCN hybrid (d). (B) Anti-fouling ability of Bi_2S_3@GCN/SPCE and its corresponding calibration plot (inset). (C) Different scan rate analysis (20 mV/s to 300 mVs) of Bi_2S_3@GCN/SPCE and corresponding calibration plot (D).

limit and excellent sensitivity, which indeed indicates that Bi_2S_3@GCN is an effective modifier for electrochemical determination of CPL (CV and DPV).

The selectivity, stability, and reproducibility of Bi_2S_3@GCN modified electrode are significant factors to be considered for real time application and analysis. There is a high probability for the presence of interfering species in real samples and therefore it is significant to evaluate the anti-interference ability of Bi_2S_3@GCN/SPCE. This electrochemical test was carried out using DPV method in the presence of various drugs, food chemicals, and biological species. In this electrochemical analysis, a high voltammetric peak response was obtained for the addition of 50 μM of CPL drug at Bi_2S_3@GCN/SPCE. Whereas, the addition of 10-fold higher concentration of interfering species such as nitroquinoline (NQ), uric acid (UA), dopamine (DA), folic acid (FA), acetaminophen (AP), nitrophenol (NP), hydrogen peroxide (HP), potassium ion (K^+), nitrobenzene (NB), sodium ion (Na^+), and glucose (Glu) exhibited only very low and negligible responses as given in Fig. 6C. Even though, CPL drug exhibits similar category chemicals as that of some interfering food chemicals and biological compounds, the interfering compounds shows less than 8% interference response.

3.7. *Storage stability and repeatability analysis of the Bi_2S_3@GCN modified sensor*

Additionally, the stability of the proposed Bi_2S_3@GCN electrode was analyzed using DPV method. Fig. 6D shows the stability performance (relative percentage) of Bi_2S_3@GCN/SPCE in presence of CPL drug over 50 days. We have observed good electrochemical performance for the proposed sensor towards CPL detection even after 50 days indicating that Bi_2S_3@GCN modified electrode has an excellent storage stability character. Moreover, the reproducibility of the Bi_2S_3@GCN modified electrode was analyzed using DPV method in presence of CPL drug (50 μM) in nitrogen gas saturated 0.05 M phaspate buffer (pH 7.0). We have fabricated 5 Bi_2S_3@GCN modified electrodes for this reproducibility

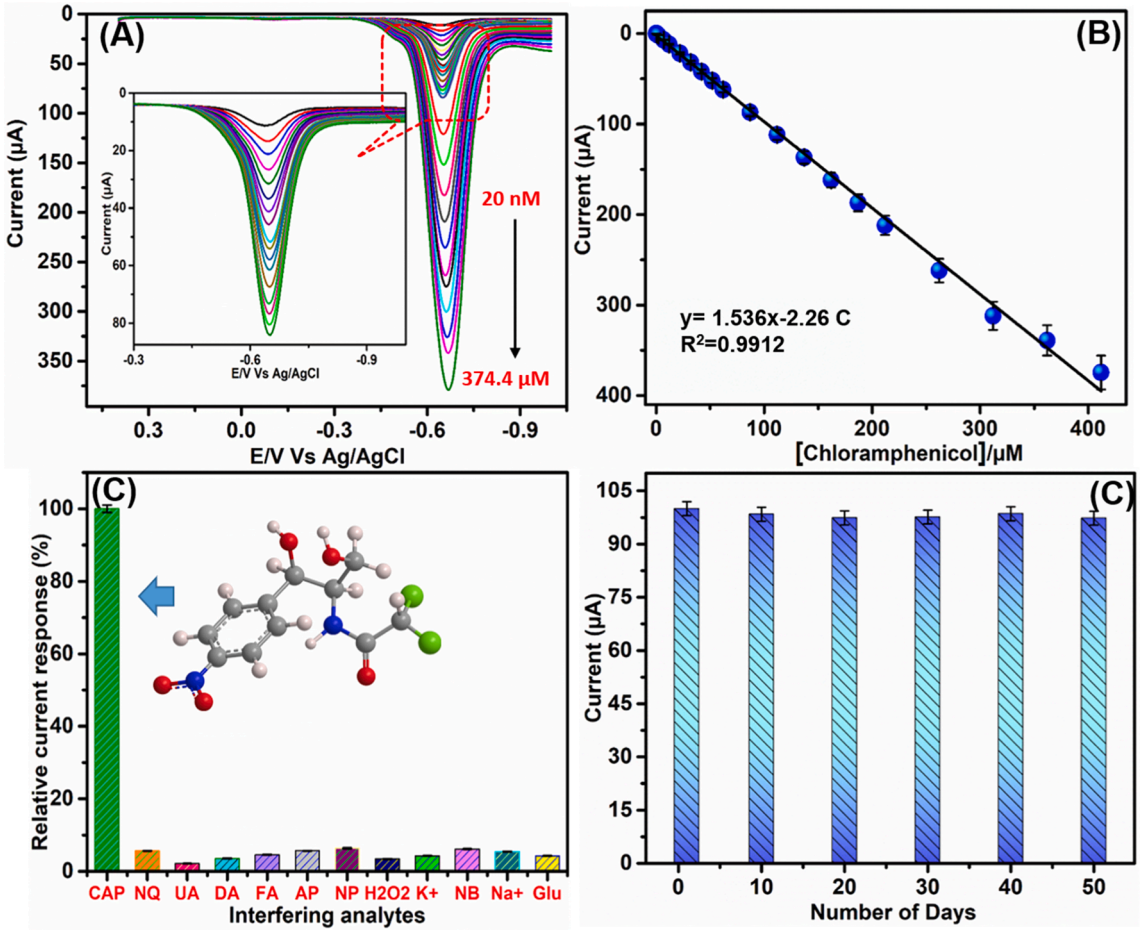

Fig. 6. (A) DPV analysis of Bi_2S_3@GCN/SPCE and its corresponding calibration plot (B). Anti-interference ability of Bi_2S_3@GCN/SPCE (C) and stability analysis of the modified sensor (D).

Table 1
Modified sensor parameters of Bi_2S_3@GCN modified electrode in presence of CPL with previously published modified electrodes.

Electrodes	Linear range (μM)	LOD (μM)	Methods	Reference
PANi NWs	–	0.0012	DPV	[40]
Fe_3O_4-CMC@Au	2.5–25	0.07	SWV	[20]
Au NPs/GrO	1.5–2.95	0.25	DPV	[41]
RGO	1–113	0.15	AM (i-t)	[42]
MoS_2/PANI	0.1–100	0.065	AM (i-t)	[43]
Porous carbon	1.0–4.0	0.0029	LSV	[44]
rGO-Pt-Pd NC	0.2–30	0.1	LSV	[45]
TiN-RGO	0.05–100	0.02	DPV	[46]
Bi_2S_3@GCN/SPCE	0.02–374.4	0.0012	DPV	This work

CMC-magnetite nanostructures stabilized with carboxymethyl cellulose, GrO-graphene oxide, MWCNT-multi-walled carbon nanotube, RGO-reduced graphene oxide, PANI-polyaniline, DPV-differential pulse voltammetry, LSV-linear sweep voltammetry.

analysis and the voltammetric responses of these modified electrodes were noted. The performance plot for reduction of CPL current vs. modified electrodes is given in Fig. 7A. According to the calibration plot, the RSD (relative standard deviation) was calculated as 3.24%. The repeatability of the Bi_2S_3@GCN/SPCE sensor was analyzed by ten repeated measurements with same electrode and the DPV method was applied in presence of CPL drug (50 μM) at a scan rate of 50 mV s^{-1} (Fig. 7B) and the RSD was calculated as 3.13%. Ultimately, the excellent performance of Bi_2S_3@GCN/SPCE sensor towards CPL drug detection was confirmed from the aforementioned investigations as it exhibited outstanding selectivity, long stability, reproducibility and repeatability.

3.8. Electrochemical determination of CPL in food samples at core–shell Bi_2S_3@GCN/SPCE by DPV

In order to evaluate the practicability of Bi_2S_3@GCN/SPCE electrode, a known concentration of CPL was spiked in fresh milk sample and was analyzed. The concentration of CPL drug was estimated from this real sample and the recovery value was noted. Moreover, a milk was diluted in phosphate buffer (pH 7.0) and the recognized concentration of CPL drug was spiked into the milk. Furthermore, the DPV analysis of Bi_2S_3@GCN modified SPCE is detected for the CPL drug-spiked milk. Similar procedure and method were applied to analyze the applicability of the sensor in shrimp extract and honey samples. The recovery values of the real sample analysis were obtained in the range of 99.02–99.80% and is given in Table 2. The electrochemical response we have obtained for this real sample analysis using DPV method was also compared with the standard method, HPLC. The excellent recovery values obtained from this experiment using both DPV and HPLC method confirms the real time applicability of the proposed Bi_2S_3@GCN/SPCE based sensor for the detection of CPL drug in food products.

4. Conclusion

The core–shell like Bi_2S_3@GCN electrocatalyst consisting of nanostars-based metal sulfide hierarchical architecture was developed based on a robust and green sonochemical approach. We have successfully and profitable performed a highly sensitive and selective electrocatalytic detection of antibiotic drug using a novel core–shell Bi_2S_3@GCN electrode materials modified SPCE. The Bi_2S_3@GCN/SPCE

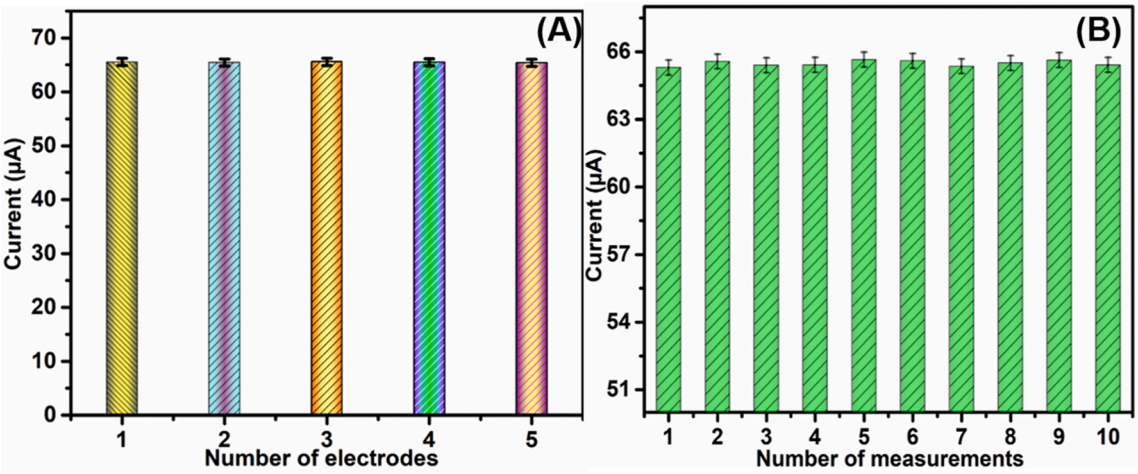

Fig. 7. (A) Sensor stability analysis of Bi_2S_3@GCN/SPCE towards CPL and reproducibility analysis of the Bi_2S_3@GCN modified sensor (D).

Table 2
Determination of CPL in food sample at Bi_2S_3@GCN/SPCE. Related standard deviation (RSD) of 3 independent experiments.

Meat Samples	Added (nM)	Found (nM)		Recovery (%)		*RSD (%), n = 3	
		i-t	HPLC	i-t	HPLC	i-t	HPLC
Fresh milk	0	0	0	–	–	–	–
	100	99.26	99.28	99.26	99.28	0.23	0.12
	200	198.41	198.62	99.20	99.31	1.62	1.08
	500	498.6	499.01	99.72	99.80	1.12	0.19
Shrimp extract	0	0	0	–	–	–	–
	100	99.12	99.36	99.12	99.36	0.26	0.14
	200	198.35	198.4	99.18	99.20	1.96	1.42
	500	497.6	498.1	99.52	99.62	0.96	0.82
Honey	0	0	0	–	–	–	–
	100	99.12	99.02	99.12	99.02	0.15	0.17
	200	496.3	496.6	99.26	99.32	0.26	0.13
	500	497.8	498.3	99.56	99.66	0.96	0.75

sensor exhibited a high sensitivity with a nanomolar detection limit of 0.0012 μM, surpassing the sensitivity of various modified electrodes reported previously. The modified SPCE based sensor has performed in the linear range of 0.02 to 374.4 μM and it exhibited long time stability, good repeatability, and reproducibility. The real-time applicability of the proposed Bi_2S_3@GCN modified sensor was demonstrated with food and food products samples. The anti-interference ability has also been analyzed with many interfering chemicals and ions. Hence, we can conclude that the proposed Bi_2S_3@GCN modified SPCE is excellent for highly sensitive and efficient determination of antibiotic drug in milk, honey, and shrimp extract samples.

Conflicts of interest

On behalf of the authors, there are no conflicts to declare.

CRediT authorship contribution statement

Mani Govindasamy: Writing - original draft, Visualization, Project administration, Resources, Methodology. **Sea-Fue Wang:** Resources, Supervision. **Albandary Almahri:** Supervision, Funding acquisition, Validation. **U. Rajaji:** Software, Visualization, Investigation.

Declaration of Competing Interest

The authors declare that they have no known competing financial interests or personal relationships that could have appeared to influence the work reported in this paper.

Acknowledgements

This work was supported by Ministry of Science and Technology (MOST-108-2221-E-027-063), National Taipei University of Technology (NTUT) through their financial encouragement.

Appendix A. Supplementary data

Supplementary data to this article can be found online at https://doi.org/10.1016/j.ultsonch.2020.105445.

References

[1] B.G. Pollet, M. Ashokkumar, Short introduction to sonoelectrochemistry, in: Introduction to Ultrasound, Sonochemistry and Sonoelectrochemistry, Springer, 2019, pp. 21–39.
[2] B.G. Pollet, The use of ultrasound for the fabrication of fuel cell materials, Int. J. Hydrogen Energy 35 (2010) 11986–12004.
[3] B.G. Pollet, M. Ashokkumar, Fundamental and applied aspects of ultrasonics and sonochemistry, in: Introduction to Ultrasound, Sonochemistry and Sonoelectrochemistry, Springer, 2019, pp. 1–19.
[4] B.G. Pollet, Let's not ignore the ultrasonic effects on the preparation of fuel cell materials, Electrocatalysis 5 (2014) 330–343.
[5] J.K. Cooper, S. Gul, F.M. Toma, L. Chen, Y.-S. Liu, J. Guo, J.W. Ager, J. Yano, I. D. Sharp, Indirect bandgap and optical properties of monoclinic bismuth vanadate, J. Phys. Chem. C 119 (2015) 2969–2974.
[6] X. Huang, S. Huang, P. Biswas, R. Mishra, Band gap insensitivity to large chemical pressures in ternary bismuth iodides for photovoltaic applications, J. Phys. Chem. C 120 (2016) 28924–28932.
[7] D.J. Riley, J.P. Waggett, K.U. Wijayantha, Colloidal bismuth sulfide nanoparticles: a photoelectrochemical study of the relationship between bandgap and particle size, J. Mater. Chem. 14 (2004) 704–708.
[8] M.R. Gao, S.H. Yu, J. Yuan, W. Zhang, M. Antonietti, Poly (ionic liquid)-mediated morphogenesis of bismuth sulfide with a tunable band gap and enhanced electrocatalytic properties, Angew. Chem. Int. Ed. 55 (2016) 12812–12816.
[9] T.J. McCarthy, T.A. Tanzer, M.G. Kanatzidis, A new metastable three-dimensional bismuth sulfide with large tunnels: synthesis, structural characterization, ion-exchange properties, and reactivity of KBi3S5, J. Am. Chem. Soc. 117 (1995) 1294–1301.
[10] Z. Zhang, C. Zhou, L. Huang, X. Wang, Y. Qu, Y. Lai, J. Li, Synthesis of bismuth sulfide/reduced graphene oxide composites and their electrochemical properties for lithium ion batteries, Electrochim. Acta 114 (2013) 88–94.
[11] Q. Lu, F. Gao, S. Komarneni, Biomolecule-assisted synthesis of highly ordered snowflakelike structures of bismuth sulfide nanorods, J. Am. Chem. Soc. 126 (2004) 54–55.
[12] M. Salavati-Niasari, D. Ghanbari, F. Davar, Synthesis of different morphologies of bismuth sulfide nanostructures via hydrothermal process in the presence of thioglycolic acid, J. Alloy. Compd. 488 (2009) 442–447.
[13] S. Cao, J. Low, J. Yu, M. Jaroniec, Polymeric photocatalysts based on graphitic carbon nitride, Adv. Mater. 27 (2015) 2150–2176.

[14] Y. Zheng, J. Liu, J. Liang, M. Jaroniec, S.Z. Qiao, Graphitic carbon nitride materials: controllable synthesis and applications in fuel cells and photocatalysis, Energy Environ. Sci. 5 (2012) 6717–6731.
[15] M.J. Bojdys, J.O. Müller, M. Antonietti, A. Thomas, Ionothermal synthesis of crystalline, condensed, graphitic carbon nitride, Chemistry 14 (2008) 8177–8182.
[16] J. Xu, L. Zhang, R. Shi, Y. Zhu, Chemical exfoliation of graphitic carbon nitride for efficient heterogeneous photocatalysis, J. Mater. Chem. A 1 (2013) 14766–14772.
[17] G. Algara-Siller, N. Severin, S.Y. Chong, T. Björkman, R.G. Palgrave, A. Laybourn, M. Antonietti, Y.Z. Khimyak, A.V. Krasheninnikov, J.P. Rabe, Triazine-based graphitic carbon nitride: a two-dimensional semiconductor, Angew. Chem. Int. Ed. 53 (2014) 7450–7455.
[18] L.G. Albano, T.P. Vello, D.H. de Camargo, R.M. da Silva, A.C. Padilha, A. Fazzio, C. C. Bufon, Ambipolar resistive switching in an ultrathin surface-supported metal-organic framework vertical heterojunction, Nano Lett. 20 (2020) 1080–1088.
[19] A. Chatzitakis, C. Berberidou, I. Paspaltsis, G. Kyriakou, T. Sklaviadis, I. Poulios, Photocatalytic degradation and drug activity reduction of chloramphenicol, Water Res. 42 (2008) 386–394.
[20] P. Jakubec, V. Urbanová, Z. Medříková, R. Zbořil, Advanced sensing of antibiotics with magnetic gold nanocomposite: electrochemical detection of chloramphenicol, Chemistry 22 (2016) 14279–14284.
[21] U. Rajaji, A. Muthumariappan, S.-M. Chen, T.-W. Chen, T.-W. Tseng, K. Wang, D. Qi, J. Jiang, Facile sonochemical synthesis of porous and hierarchical manganese (III) oxide tiny nanostructures for super sensitive electrocatalytic detection of antibiotic (chloramphenicol) in fresh milk, Ultrason. Sonochem. 58 (2019).
[22] M. Govindasamy, S.-M. Chen, V. Mani, R. Devasenathipathy, R. Umamaheswari, K. J. Santhanaraj, A. Sathiyan, Molybdenum disulfide nanosheets coated multiwalled carbon nanotubes composite for highly sensitive determination of chloramphenicol in food samples milk, honey and powdered milk, J. Colloid Interface Sci. 485 (2017) 129–136.
[23] V. Mani, T. Balamurugan, S.-T. Huang, Rapid one-pot synthesis of polydopamine encapsulated carbon anchored with au nanoparticles: versatile electrocatalysts for chloramphenicol and folic acid sensors, Int. J. Mol. Sci. 21 (2020) 2853.
[24] J.C. Hanekamp, A. Bast, Antibiotics exposure and health risks: chloramphenicol, Environ. Toxicol. Pharmacol. 39 (2015) 213–220.
[25] X.-B. Chen, Y.-L. Wu, T. Yang, Simultaneous determination of clenbuterol, chloramphenicol and diethylstilbestrol in bovine milk by isotope dilution ultraperformance liquid chromatography–tandem mass spectrometry, J. Chromatogr. B 879 (2011) 799–803.
[26] P. Hughes, J. Heritage, Antibiotic growth-promoters in food animals, FAO Animal Production and Health Paper, (2004) 129-152.
[27] J.C. Hanekamp, J.H. Kwakman, Towards intended normal use (part I): a European appraisal of the chloramphenicol case and some thoughts on the potential of global harmonization of antibiotics regulation, Ensuring Global Food Safety, Elsevier (2010) 193–208.
[28] J. Ferguson, A. Baxter, P. Young, G. Kennedy, C. Elliott, S. Weigel, R. Gatermann, H. Ashwin, S. Stead, M. Sharman, Detection of chloramphenicol and chloramphenicol glucuronide residues in poultry muscle, honey, prawn and milk using a surface plasmon resonance biosensor and Qflex® kit chloramphenicol, Anal. Chim. Acta 529 (2005) 109–113.
[29] R. Levi, S. McNiven, S.A. Piletsky, S.-H. Cheong, K. Yano, I. Karube, Optical detection of chloramphenicol using molecularly imprinted polymers, Anal. Chem. 69 (1997) 2017–2021.
[30] T. Nagata, H. Oka, Detection of residual chloramphenicol, florfenicol, and thiamphenicol in yellowtail fish muscles by capillary gas chromatography–mass spectrometry, J. Agric. Food. Chem. 44 (1996) 1280–1284.
[31] P. Gonzalez-Rodriguez, K.J. van den Nieuwenhuijzen, W. Lette, D.J. Schipper, J. E. ten Elshof, Tribochemistry of bismuth and bismuth salts for solid lubrication, ACS Appl. Mater. Interfaces 8 (2016) 7601–7606.
[32] T. Fazal, B. Ismail, S. Wafee, A. Kambooh, A. Khan, Cu doped Bi2S3 as potential absorbers for thin film solar cells: optical and structural properties, Chalcogenide Lett. 13 (2016) 225–231.
[33] F. Fina, S.K. Callear, G.M. Carins, J.T. Irvine, Structural investigation of graphitic carbon nitride via XRD and neutron diffraction, Chem. Mater. 27 (2015) 2612–2618.
[34] Y. Huang, W. Fan, B. Long, H. Li, F. Zhao, Z. Liu, Y. Tong, H. Ji, Visible light Bi2S3/Bi2O3/Bi2O2CO3 photocatalyst for effective degradation of organic pollutions, Appl. Catal. B 185 (2016) 68–76.
[35] Y. Wang, W. Tian, L. Chen, F. Cao, J. Guo, L. Li, Three-dimensional WO3 nanoplate/Bi2S3 nanorod heterojunction as a highly efficient photoanode for improved photoelectrochemical water splitting, ACS Appl. Mater. Interfaces 9 (2017) 40235–40243.
[36] F. Qiao, J. Wang, S. Ai, L. Li, As a new peroxidase mimetics: The synthesis of selenium doped graphitic carbon nitride nanosheets and applications on colorimetric detection of H2O2 and xanthine, Sens. Actuators, B 216 (2015) 418–427.
[37] S. Gu, J. Xie, C.M. Li, Hierarchically porous graphitic carbon nitride: large-scale facile synthesis and its application toward photocatalytic dye degradation, RSC Adv. 4 (2014) 59436–59439.
[38] U. Rajaji, T.-W. Chen, S. Chinnapaiyan, S.-M. Chen, M. Govindasamy, Two-dimensional binary nanosheets (Bi2Te3@ g-C3N4): application toward the electrochemical detection of food toxic chemical (Ractopamine), Anal. Chim. Acta (2020).
[39] T. Alizadeh, M.R. Ganjali, M. Zare, P. Norouzi, Selective determination of chloramphenicol at trace level in milk samples by the electrode modified with molecularly imprinted polymer, Food Chem. 130 (2012) 1108–1114.
[40] T.-X. Chu, V.-P. Vu, H.-T. Tran, T.-L. Tran, Q.-T. Tran, T. Le Manh, Molecularly imprinted polyaniline nanowire-based electrochemical biosensor for chloramphenicol detection: a kinetic study of aniline electropolymerization, J. Electrochem. Soc. 167 (2020).
[41] R. Karthik, M. Govindasamy, S.-M. Chen, V. Mani, B.-S. Lou, R. Devasenathipathy, Y.-S. Hou, A. Elangovan, Green synthesized gold nanoparticles decorated graphene oxide for sensitive determination of chloramphenicol in milk, powdered milk, honey and eye drops, J. Colloid Interface Sci. 475 (2016) 46–56.
[42] X. Zhang, Y.-C. Zhang, J.-W. Zhang, A highly selective electrochemical sensor for chloramphenicol based on three-dimensional reduced graphene oxide architectures, Talanta 161 (2016) 567–573.
[43] R. Yang, J. Zhao, M. Chen, T. Yang, S. Luo, K. Jiao, Electrocatalytic determination of chloramphenicol based on molybdenum disulfide nanosheets and self-doped polyaniline, Talanta 131 (2015) 619–623.
[44] L. Xiao, R. Xu, Q. Yuan, F. Wang, Highly sensitive electrochemical sensor for chloramphenicol based on MOF derived exfoliated porous carbon, Talanta 167 (2017) 39–43.
[45] F.-Y. Kong, Y. Luo, J.-W. Zhang, J.-Y. Wang, W.-W. Li, W. Wang, Facile synthesis of reduced graphene oxide supported Pt-Pd nanocubes with enhanced electrocatalytic activity for chloramphenicol determination, J. Electroanal. Chem. 781 (2016) 389–394.
[46] F.-Y. Kong, T.-T. Chen, J.-Y. Wang, H.-L. Fang, D.-H. Fan, W. Wang, UV-assisted synthesis of tetrapods-like titanium nitride-reduced graphene oxide nanohybrids for electrochemical determination of chloramphenicol, Sens. Actuators, B 225 (2016) 298–304.